ACS OMEGA

Open Access

http://pubs.acs.org/journal/acsodf

Article

Monodispersed Bubble Generation Using Hydrophobic Orifices: The Extended Tate's Law

Bo Liu,* Hao Zhang, Haiqiang Yang, Fang Yuan, and Qiang Yang*

Cite This: *ACS Omega* 2024, 9, 18854−18861

Read Online

ACCESS | Metrics & More | Article Recommendations | Supporting Information

ABSTRACT: The use of submerged orifices for bubble generation is ubiquitous in industries with wettability known to influence the bubble departure diameter. In this study, we investigated bubble generation and departure from the orifices (0.3−2 mm) drilled on hydrophobic perfluoroalkoxy (PFA) tubes in water. By varying the gas inflow rate (33 to 200 mL/min), we found that the Sauter mean diameter closely matched those generated by hydrophilic quartz orifices. However, monodispersed bubbles were formed on the PFA tube compared to those on quartz with much wider size distributions. By examining the dynamic bubbling process, we confirmed its agreement with Tate's law, which was originally developed for quasi-steady conditions and emphasizes a balance between capillary and buoyancy forces. However, it should be noted that dynamic conditions lead to an increase in bubble volume compared to the quasi-steady condition despite following the same principle, which is explained by the continuous gas inflow when the bubble departs from the orifice at a necking stage. The above understandings enable generation of monodispersed bubbles under dynamic conditions, benefiting industries requiring precise control on bubble size, such as the bubble assisted wet etching and cleaning processes in semiconductor fabrication.

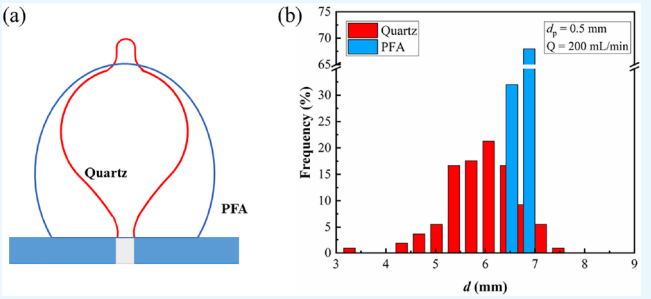

1. INTRODUCTION

The utilization of orifices for bubble generation at liquid phase is extensively employed in various industries, including chemical, metallurgical, and nuclear sectors.[1−5] In such processes, precise control of bubble diameter is often crucial as it directly impacts the bubble's ascent rate, motion behavior, as well as mass and heat transfer characteristics. For example, the size of generated helium bubbles is crucial for the removal of gaseous fission product 135 Xe from the circulating fuel in a molten salt nuclear reactor.[6−8] Another prime illustration of this concept can be found in the bubble-assisted wet etching-cleaning process employed in semiconductor fabrication. In such contexts, the meticulous regulation of bubble size becomes crucial to ensure consistent and uniform fabrication across numerous substrates within a batch.[9,10] However, the growth and detachment of bubbles from orifices are influenced by numerous factors, including operating parameters (such as gas velocity and pressure), system parameters (such as orifice size and material), and fluid characteristics (such as surface tension and liquid viscosity). The interplay of these factors is intricate and comprehensive research in this field is still ongoing, leaving certain aspects yet to be fully explored.[11−15]

One theoretical approach to predict bubble diameter generated by orifices is Tate's law. Credited to Tate in 1864,[16] this model was initially proposed to explain the formation of liquid droplets from a needle, and has been extensively validated and employed for determining surface tension of liquid phase.[17−19] The model can also be used to predict the bubble detachment from an orifice, because of the similarity between bubbles and drops. For bubbles, the model predicts their detachment from the orifice once the buoyancy force exceeds the maximum capillary force, which is written as $\Delta\rho gV = \pi d_p\sigma$, where $\Delta\rho$ is the density difference between the gas phase and the liquid phase (kg/m^3), g is the gravitational acceleration (m/s^2), V is the volume of the droplet (bubble, m^3), d_p is the diameter of the orifice (capillary, m), and σ is the surface tension (N/m).[20,21] Therefore, with the known information on the orifice size and surface tension, the bubble detachment can be precisely controlled, i.e., monodispersed bubble/drops are expected. The model predicts the one-to-one correspondence between orifice diameter d_p and bubble diameter d, as shown in Figure 1b.

Despite the success of Tate's law, applying this theory to industrial bubbling conditions reveals clear limitations.[12,18,22] The assumption of quasi-steady gas injection clearly deviates from industrial settings, where continuous gas injection at specific flow rates is necessary. Increased gas flow rates introduce hydrodynamic forces such as the added mass effect

Received: October 18, 2023
Revised: February 29, 2024
Accepted: April 10, 2024
Published: April 17, 2024

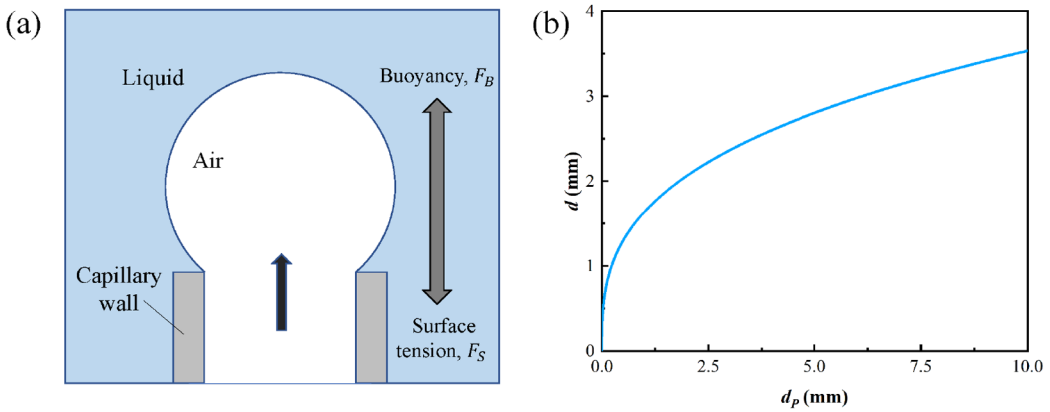

Figure 1. (a) Force balance during bubble formation at a submerged orifice based on Tate's law. (b) The bubble-orifice size relationship as predicted by Tate's law.

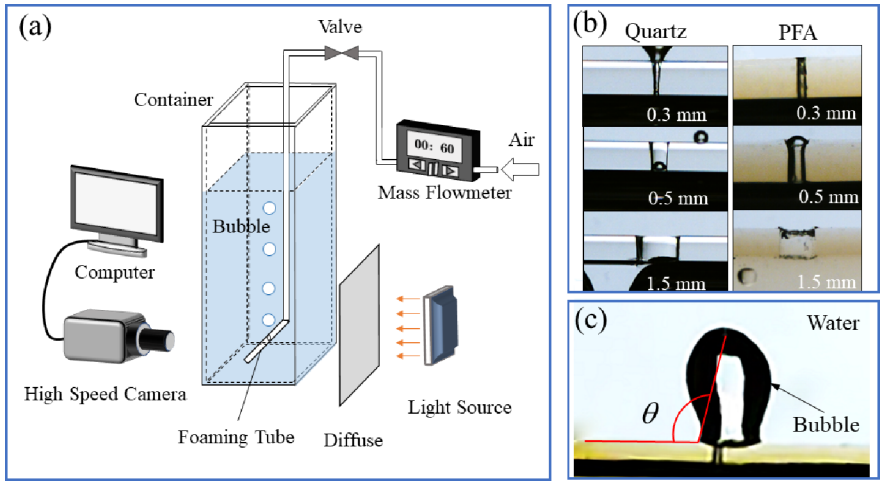

Figure 2. (a) Schematic illustration of the experimental system for bubble generation and image acquisition. (b) Images of the orifices drilled on two kinds of tubes. (c) Illustration of the contact angle of the PFA tube; note that the contact angle is a dynamic value that evolves with bubble size and the advancing/receding of the three-phase contact line.

arises from the acceleration of growing bubbles,[1] challenging Tate's law's application further.[23,24] Additionally, coalescence of bubbles affects size distribution, deviating from the theory's predictions of single sized bubbles. Moreover, the one-to-one correspondence between bubble size and orifice size restricts the flexibility in designing multiorifice bubble generators. Achieving equal gas distribution at different orifices and forming relatively large bubbles becomes challenging, as small orifices favor equal gas distribution.[25] Addressing these limitations and understanding the interplay between gas flow, orifice size, and bubble generation is crucial for effectively applying Tate's law in industrial contexts.

The use of nonwetting surfaces for bubble generation has gained increasing attention due to their ability to enlarge bubble size without increasing the orifice size.[2,11,26] Nonwetting surfaces facilitate the spreading of the gas−liquid−solid contact line, resulting in a larger contact area between the bubble and surface compared to wetted surfaces.[27,28] This leads to a substantial increase in the capillary force that retains the bubbles at the orifice. Experimental studies by Lin et al.[28] demonstrate that increasing the contact angle from 45° to 100° can cause the bubble volume to increase 10-fold or more. Additionally, Mirsandi et al.[11] found that surface roughness and heterogeneity play a significant role in affecting contact line movement. These findings were primarily obtained for bubbles generated at a low gas flow rate of about 10 mL/min. As the gas flow rate increases, the influence of wettability on bubble generation becomes less significant,[5,11] which diminishes the importance of selecting nonwetting surfaces for bubble generation.

In this work, we explore an additional feature of bubble generation from a hydrophobic PFA surface: the size distribution, unveiling the advantages of nonwetted surfaces in producing monodispersed bubbles. A series of experiments were conducted using a transparent rectangular container and two types of tubes, namely, PFA and quartz, to investigate and compare the bubble growth and detachment processes, considering their distinctly different wettability. At gas flow rates of up to 200 mL/min, we observed similar bubble sizes but a clear distinction in bubble size distribution between the two tubes. The generation of monodispersed bubbles using hydrophobic PFA tubes at high gas flow rates was revealed, and the underlying mechanism was discussed based on experimental observations and theoretical considerations.

2. MATERIALS AND METHOD

2.1. Experimental Section. The experimental setup, as illustrated in Figure 2a, was conducted within a rectangular

https://doi.org/10.1021/acsomega.3c08187
ACS Omega 2024, 9, 18854−18861

acrylic tank measuring 100 × 100 mm (length) × 100 × 600 mm (height). The top portion of the tank was open to the atmosphere, and an L-shaped foam tube was securely fixed inside the tank for bubble generation. In this study, air served as the dispersed phase, while deionized water acted as the continuous phase. The air was introduced into the tube through an air compressor (1400W-30L, SENSETER), and the flow rate was regulated using an electronic flowmeter (SLD-MFC, SENLOD) before entering the tube, where bubble generation occurred at the orifice. All experiments were conducted at room temperature, with gas flow rates ranging from 33 to 200 mL/min. A high-speed camera (FASTCAM Mini AX100, Photron. Ltd.) was used for image acquisition. The acquisition frequency was 1000 fps, the shutter speed is 1/10000 s, and the resolution was 1024 × 1024 pixels. Illumination for the high-speed camera area was provided by a LED lamp behind the tank.

The experimental setup involved the use of two types of foam tubes: one made of quartz and the other made of PFA (as depicted in Figure 2b). Both of them had an inner diameter of 4 mm and a wall thickness of 1 mm. Among them, PFA stands out for its remarkable hydrophobic properties, effectively repelling water and exhibiting a relatively high contact angle with water (contact angle $\theta \approx 110°$, as illustrated in Figure 2c). On the other hand, the contact angle of quartz material is intricately tied to the cleaning method used, often resulting in a contact angle of less than 40° after undergoing appropriate treatment.[29−31] It should be noted that the contact angle mentioned here is a dynamic value that evolves with bubble size and the advancing/receding of the three-phase contact line. Different aperture sizes were set for the experiment, namely, 0.3 0.5, 1, 1.5, and 2.0 mm. Detailed parameters can be found in Table 1. At the flow rate of 200 mL/min, the orifice

Table 1. Aperture Sizes and Experimental Parameters were Used in this Study

aperture (mm)		0.3	0.5	1	1.5	2
orifice gas velocity (m/s)	33 mL/min	7.78	2.8	0.7	0.31	0.18
	66 mL/min	15.56	5.6	1.4	0.62	0.35
	100 mL/min	23.58	8.49	2.12	0.94	0.53
	133 mL/min	31.36	11.29	2.82	1.25	0.71
	166 mL/min	39.14	14.09	3.52	1.57	0.88
	200 mL/min	47.16	16.98	4.24	1.89	1.06

gas velocity v would reach 16.98 and 47.16 m/s for 0.5 and 0.3 mm orifices, respectively, providing that the gas flows through the orifice at a constant rate. This high velocity flow would contribute to a pressure of more than 100 Pa at the top bubble surface as estimated from the Bernoulli equation $p_{add} \sim \rho v^2/2$, the added pressure p_{add} is at the same order of magnitude of the Laplace pressure ($4\sigma/d_p \approx 50$ Pa), and would affect the bubble shape. The added pressure can be even more significant considering that the gas flow through the orifice typically occurs in a periodical manner.[25]

2.2. Image Analysis and Data Processing. The original images captured by the high-speed camera are in the RGB color format (Figure 3a). The images were processed using the following steps. First, each image was converted from RGB to grayscale format (Figure 3b). The contrast of the image was further enhanced by adjusting the color balance (Figure 3c). Afterward, the image was binarized (Figure 3d) and the hole inside the bubble was filled (Figure 3e) before the bubble edge was detected (Figure 3f) for data analysis.

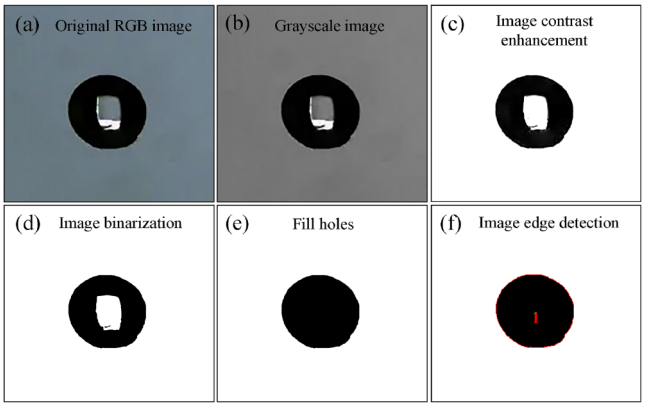

Figure 3. Steps of image processing using ImageJ software: (a) original image acquisition, (b) image conversion to gray scale, (c) image contrast enhancement and (d) image binarization, (e) fill holes, and (f) image edge detection.

3. RESULTS AND DISCUSSION

Figure 4 provides a sequence of snapshots to illustrate the bubble growth process from the tubes made from both quartz and PFA. The experiments were conducted at a volumetric flow rate of 200 mL/min and the orifice diameter of 0.5 mm for both tubes. Figure 4a depicts the bubbling process using the quartz tube, where the three-phase contact line of the growing bubble remains adhered to the inner edge of the orifice and does not vary during the growth process, which agrees with the observations of Lin et al.[28] Notably, due to the presence of a protruding tip at the top of the growing bubble, the growing bubble tends to coalesce with the just detached bubble, resulting in the formation of larger bubbles. As mentioned previously, the protruding tip results from p_{add}. It should be noted that bubble coalescence rarely occurs when the orifice diameter is larger than 0.75 mm. This can be attributed to the reduced orifice gas velocity and the significantly decreased p_{add} since $p_{add}\alpha\ v^2\alpha\ d^{-4}$ considering that $v = Q/A = 4Q/(\pi d_p^2$, thus a spherical bubble shape can be maintained with the increase in orifice diameter.

The bubble growing on a PFA orifice exhibits two distinct differences compared to quartz: the moving three-phase contact line and the spherical bubble shape. As shown in Figure 4b, the three-phase contact line of the growing bubble expands beyond the orifice owing to the hydrophobic nature of the PFA material, leading to a much larger contact area compared to the orifice diameter, which agrees with reports by Fritz[27] and Lin et al.[28] Consequently, the capillary force retaining the bubbles at the orifice can be much larger, considering $F_s \sim \pi\phi\sigma$ rather than $\pi d_p\sigma$, where ϕ represents the diameter of the contact surface (m). As a result, the bubble volume increases proportionally to the growth of the contact area, rendering the diameter of the orifice less influential on the bubble size. Furthermore, on the PFA tube, the top of the growing bubble exhibits a smooth spherical surface. The less significant impact of gas velocity-induced pressure in this case may be attributed to the much larger inflow area at the bottom

https://doi.org/10.1021/acsomega.3c08187
ACS Omega 2024, 9, 18854−18861

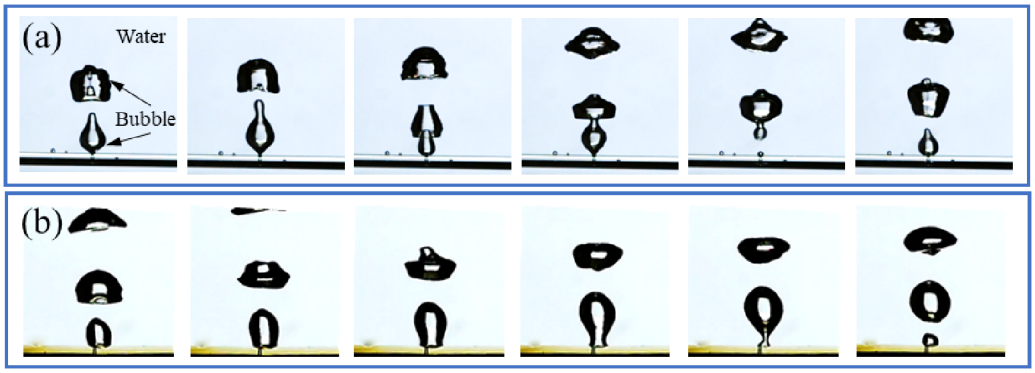

Figure 4. Snapshots of bubble growth on two tubes: (a) quartz, and (b) PFA. Gas volume flow rate Q = 200 mL/min, and orifice diameter d_p = 0.5 mm. (The deformation of the growing bubble and its coalescence with the just detached bubble is clearly visible with the quartz tube but not with the PFA tube.)

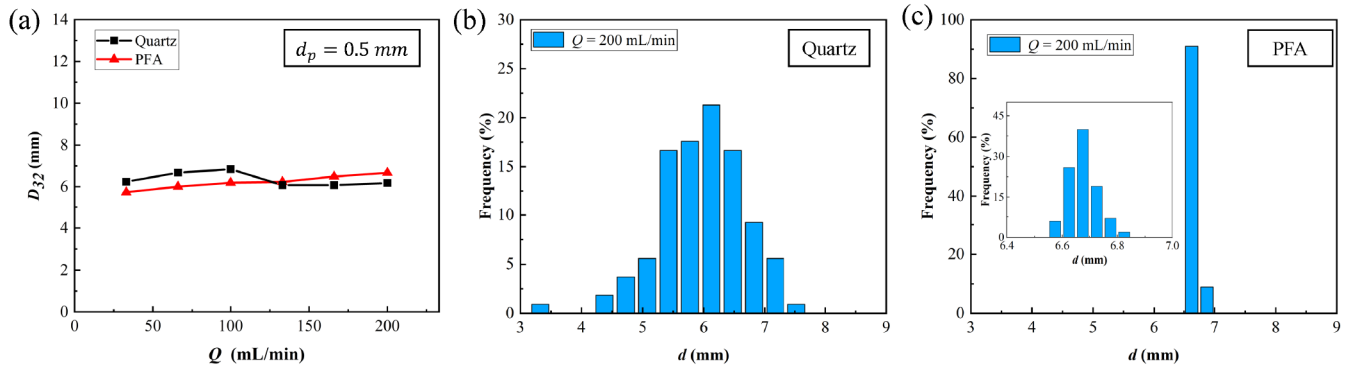

Figure 5. (a) The Sauter mean diameter D_{32} of bubbles generated by two tubes with the orifice diameter of 0.5 mm. Size distribution of bubbles obtained by two kinds of tubes (Q = 200 mL/min, d_p = 0.5 mm): (b) quartz tubes and (c) PFA tubes.

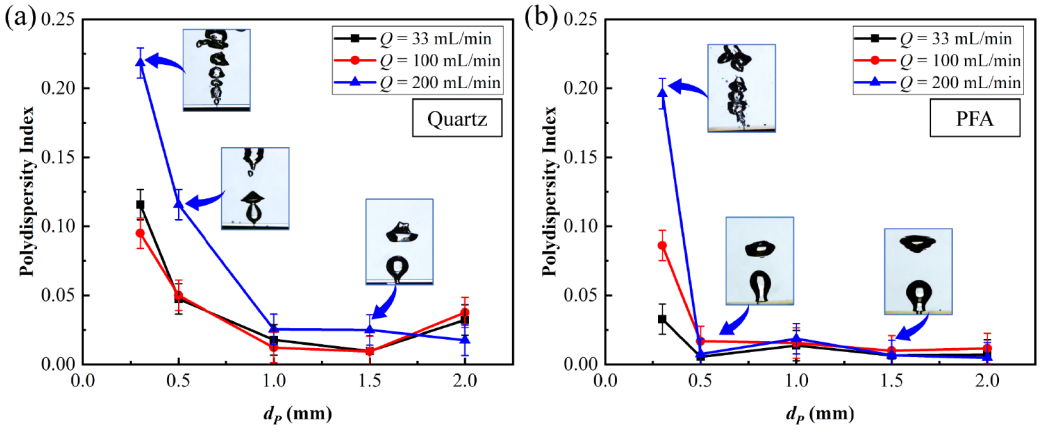

Figure 6. Polydispersity index of bubble diameter for bubbles generated by two tubes: (a) quartz tubes and (b) PFA tubes, at different orifice diameters and gas flow rates.

of the PFA tube compared with the quartz tube. Overall, the growth and detachment of the bubble exhibit a highly reproducible pattern, and coalescence between subsequent bubbles is not observed, except when the orifice is reduced to 0.3 mm (see Supporting Information).

Figure 5 describes the bubble size distribution under the two materials. As shown in Figure 5a, the Sauter mean diameter (D_{32}) of bubbles under two conditions is very close to that of two materials at an orifice diameter of 0.5 mm. More specifically, D_{32} ranges from 6 to 7 mm in both cases. For PFA, D_{32} experiences a gradual increase with volumetric flow rate, while the evolution behavior is not clear for quartz. At a flow rate of 200 mL/min, D_{32} = 6.18 mm under a quartz tube and D_{32} = 6.67 mm under the PFA tube.

Despite the close D_{32}, the bubble size distribution generated by the two tubes can be quite different. As shown in Figure 5b, the bubble size presents a wide distribution range between 3.5 and 7.5 mm with a quartz tube. In contrast, Figure 5c depicts an almost monodispersed bubble size distribution range between 6.5 and 7 mm using PFA tubes. On one hand, the discovery reaffirms the limited impact of materials on the mean bubble size within dynamic bubbling systems, providing

https://doi.org/10.1021/acsomega.3c08187
ACS Omega 2024, 9, 18854−18861

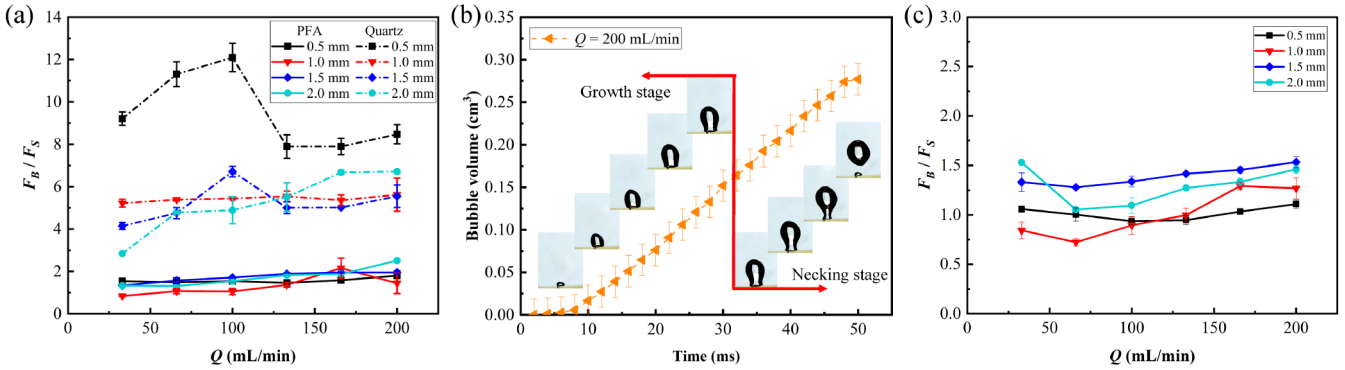

Figure 7. (a) The ratio between buoyance force and capillary force for bubbles generated by quartz and PFA tubes. (b) Two stages of bubble growth (Q = 200 mL/min, d_p = 0.5 mm): expansion stage without neck formation (capillary force dominant) and exit stage with neck shrinkage and detachment. (c) Ratio of buoyancy to capillary force using bubble size at the transition point between the two stages.

flexibility in selecting orifice materials for bubble generation. On the other hand, this finding presents a novel opportunity and capability to produce bubbles with meticulous control, allowing for not only a focus on the mean size but also on the distribution of bubble sizes. The variation in the bubble size distribution for two materials can be attributed to differences in the bubble generation process. As seen in Figure 4, bubbles produced by the quartz tube undergo coalescence behavior after separation, leading to the formation of larger bubbles through the merging of smaller ones. On the other hand, the large bubbles generated by the PFA tube directly grow without undergoing coalescence. This finding aligns with the results of Corchero et al.,[2] where they observed that as the static contact angle changes from 90° to 120°, the bubble expands toward the surface of the orifice plate during its growth, resulting in a volume increase of up to 2.34 times under nonwetting conditions.

To assess the uniformity of bubble size, the polydisperse index (PDI) was calculated for bubbles under both conditions.[32] The polydispersity index is defined as the standard deviation of the bubble radius divided by the mean radius, i.e.

$$\mathrm{PDI} = S_n/d_m \tag{1}$$

where S_n is the standard deviation of the bubble radius (m) and d_m is the average diameter of the bubble (m). A lower polydispersity index indicates a higher level of monodispersity among the bubbles.

The difference in the PDI of the bubbles generated by the two tubes is clearly visible. As shown in Figure 6, the PDI of bubble size decreases in both tubes as the orifice size increases. For quartz tubes (Figure 6a), the PDI may reach 0.22 at the orifice diameter of 0.3 mm and gradually reduces to 0.10 at the orifice diameter of 0.5 mm. It further decreases to around 0.03 at orifice diameters exceeding 0.75 mm, where bubble coalescence diminishes. For PFA tubes (Figure 6b), the PDI is around 0.015 when the orifice diameter reaches 0.5 mm, indicating the generation of monodispersed bubbles. As expected, the PDI would rise dramatically to 0.20 with the onset of bubble coalescence, as demonstrated at an orifice diameter of 0.3 mm.

The highly reproducible monodispersed bubble generation using PFA tubes is similar to the prediction of Tate's law, a theory developed for quasi-steady bubble generation. To evaluate the applicability of Tate's law at this dynamic bubbling scenario, we divided the buoyancy force of the detached bubbles by the capillary force arising from the three-phase contact line. The buoyancy force is calculated from the bubble size by using the relationship $F_b = \Delta\rho g V$. The capillary force is evaluated by considering the length of three-phase contact line, i.e., $F_s = \pi d_p \sigma$ for hydrophilic Quartz glass, and $F_s = \pi\phi\sigma$ for hydrophobic PFA tubes. The influence of the contact angle effect on the capillary force with the PFA tube should be acknowledged. However, we did not consider it due to the challenge in assigning it a specific value, as mentioned earlier. Moreover, its impact on the overall force is minimal, given that the typical contribution of the contact angle, sin110° = 0.94, is only 6% different from sin 90°, which is the value used in the calculation. The tube curvature would affect the length of the three-phase contact line, thereby affecting the evaluation of the capillary force. However, we did not factor it in due to its minimal influence, resulting in some uncertainties remaining regarding capillary force.

As shown in Figure 7a, the ratio of buoyancy to capillary forces consistently exceeds 4 for quartz tubes, while it remains below 2 for PFA tubes. The value 4 is quite reproducible for quartz tubes except for the orifice with a diameter of 0.5 mm, where the ratio reaches a value of around 8. The double relationship agrees with the experimental observation that the final size of the bubble generated by 0.5 mm orifices is achieved by the coalescence of two bubbles. The high ratio of 4 can be attributed to the dynamic bubbling behavior that the inertia of bubble growth may play a role[24], which cannot be ignored once the gas flow rate exceeds around 40 mL/min for an orifice of 0.3 mm at the air−water system.[25] These results clearly deviate from Tate's law, and the underlying mechanism responsible for this discrepancy is undoubtedly intricate. We are not attempting to explain it quantitatively here since it falls beyond the scope of the current work.

For PFA tubes, the ratio between buoyancy force and capillary force ranges between 1 and 2 across various orifice sizes, suggesting its close relation with Tate's law. It should be noted that the inertial force is still negligible for this process according to the model[24], therefore the bubbling feature is still dominated by the balance of buoyance force and capillary force, just as that assumed in Tate's law. More specifically, for the hydrophobic tubes with a contact angle of around 100°, the criteria between quasi-steady and dynamic bubbling increase to around 222 mL/min for an orifice of 0.3 mm at the air−water system,[25] and should be even higher with the increase of orifice diameter. Therefore, the expansion of the three-phase contact line significantly enhances the capillary force that retains the

https://doi.org/10.1021/acsomega.3c08187
ACS Omega 2024, 9, 18854−18861

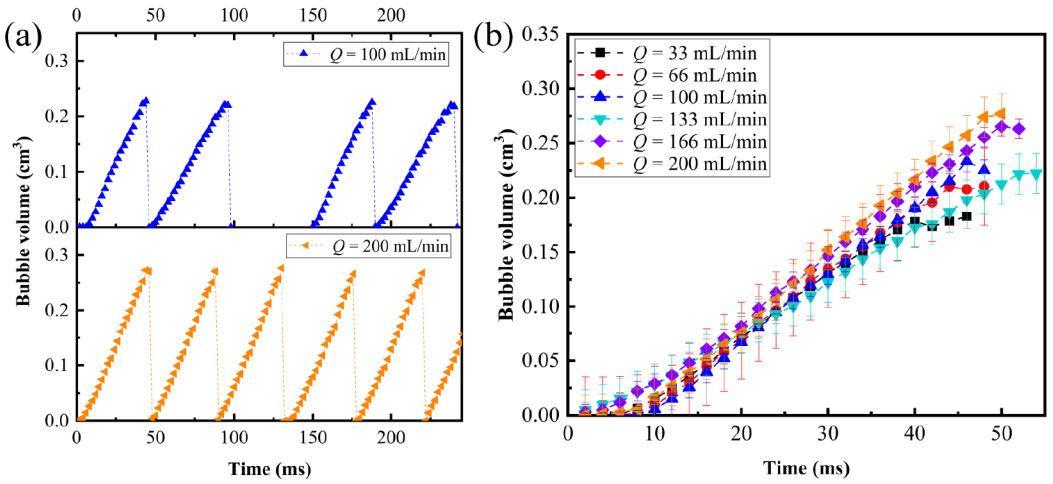

Figure 8. (a) The time evolution of bubble volume, highlighting the delay between the detachment of one bubble and the formation of the next bubble; (b) volume changes of bubbles at different gas flow rates during the growth stage.

bubble at the orifice, allowing for the sustained growth of larger bubbles. Monodispersed bubbles can be generated as expected from Tate's law.

However, it should be emphasized that the buoyancy force remains almost 2 times higher than the capillary force, suggesting that the bubble size is still 1−2 times larger than the predicted values of Tate's law. This discrepancy cannot be simply explained by the uncertainties in the evaluation of the capillary force.

Upon revisiting the experimental observations, we found that the bubble generation can be divided into two stages: the expansion stage and the exit stage, which contribute almost equally to the bubble volume under the current experimental condition. The process is depicted in Figure 7b, which shows the increase in bubble volume over a 50 ms period. During the initial stage, until approximately 30 ms, the bubble expands without the formation of a neck, indicating that the capillary force is sufficient to hold the bubble at the tube surface. With the further increase of bubble size, the neck forms and continues to shrink until its breakage; i.e., the bubble detaches from the orifice. This shrinkage process lasts another 20 ms before bubble detachment.

In this process, the bubble detachment is determined by the balance between capillary force and buoyancy force, adhering to Tate's law. The difference from typical Tate's law is that the bubble continues to grow at the exit stage, contributing roughly an additional 50% to the overall volume (from 0.16 to 0.32 cm^3) to the detached bubble. The perturbation caused by liquid inflow at the exit stage has also been reported by Kumar and Kuloor[1] in bubble generation with hydrophilic surfaces, a widely discussed feature to avoid in surface tension measurements using the drop weight method.[33]

With the hydrophobic PFA tube, the expanded three-phase contact line resulted in a wider neck compared to hydrophilic surfaces, prolonging the duration of the necking stage and allowing an additional gas to flow into the bubble, thereby increasing its final size. To confirm the reliability of this argument, we calculated the ratio between buoyancy force and capillary force using the bubble size at the transition point between stages (see Figure 7c). As expected from Tate's law, the ratio falls within a range very close to 1. Hence, we can conclude that the bubble volume is jointly determined by the two stages, and Tate's law remains the determining factor affecting the bubble volume. While features such as the monodispersed bubble generation are expected, its prediction of the bubble departure size should be augmented considering the liquid flow at the exit stage.

The explanation provided above successfully clarifies the force-determined bubble detachment using hydrophobic tubes under specific experimental conditions. However, when the impact of volumetric gas flow rate on bubble size is evaluated, a discrepancy arises. As described, the expansion stage is primarily influenced by surface properties rather than gas rate; therefore, the bubble volume at the end of this stage should be relatively constant and not severely affected by the gas flow rate. In contrast, gas inflow at the exit stage is expected to be significantly affected by the gas flow rate. The duration of the exit stage, mainly determined by necking shrinkage and breakage processes governed by surface energy and capillary flow, should remain roughly constant, regardless of the gas flow rate. Therefore, this constant bubble exit time should lead to larger bubble volumes with higher gas flow rates. However, contrary to this expectation, Figure 5 shows that the bubble size at different flow rates does not vary significantly.

The discrepancy can be explained by the fact that the gas flow through the orifice is not constant; there is a delay between the detachment of one bubble and the formation of the next (Figure 8a). This delay is a characteristic feature of bubble generation systems operating in the constant flow regime. At this regime, the gas flow into the tube is constant but not from the orifice. The bubble cannot grow from the orifice until the Laplace pressure of the small nuclei is overcome, exhibiting a delay in bubble generation. During the delay period, the pressure inside the tube steadily rises due to the accumulated gas. Once the Laplace pressure is surpassed and the bubble begins to grow, its flow rate is determined by the pressure difference resulting from the flow resistance through the orifice and the varying Laplace pressure corresponding to the instantaneous bubble size. With the release of gas from the tube to the outside, the pressure inside the tube is reduced, resulting in a slowing down of the gas flow through the orifice, i.e., the growth of bubble volume.

As shown in Figure 8a, increasing the gas flow rate reduces the delay time, thereby improving the frequency of bubble formation but does not severely affect the amount of gas flowing into the bubble during each cycle (Figure 8b).

https://doi.org/10.1021/acsomega.3c08187
ACS Omega 2024, 9, 18854−18861

Furthermore, the bubble volume evolution at different gas flow rates clearly shows a reduction in gas flow rate at the exit stage. This reduction aligns with the argument of decreased pressure in the tube. It is more pronounced at low flow rates and becomes less significant at high flow rates, possibly due to a smaller decrease in pressure with the faster inflow gas.

With the insights gained from our analysis, we can achieve a better understanding of bubble generation by using orifices. Hydrophobic surfaces enable the production of monodispersed bubbles across a wide range of gas flow rates. By transitioning from a constant flow rate regime to a constant pressure regime, for instance, using a larger chamber instead of a tube, we may facilitate the generation of larger bubbles by increasing the gas flow rate at the exit stage. Additionally, precise control of bubble size can be attained through modifications in factors such as wettability and contact angle heterogeneity. These findings offer valuable guidance for optimizing bubble generation processes in various applications. It is important to highlight that the precise bubble detachment diameter can also be influenced by various parameters, including contact angles, tube diameter, and surface roughness. As depicted in Figure 7c, the ratio of buoyancy to capillary force, based on the bubble size at the transition point between two stages, does not perfectly reach 1. This discrepancy indicates potential uncertainties attributed to the parameters mentioned earlier, underscoring the need for further investigations to better understand their effects.

4. CONCLUSIONS

In this experimental study, we investigated the growth and detachment of bubbles from a hydrophobic PFA tube orifice. Surprisingly, we observed the generation of monodispersed bubbles at a volumetric flow rate of 200 mL/min, a gas flow rate that deviates significantly from quasi-steady conditions. By analyzing the volume of detached bubbles and considering the local contact with the expanding three-phase contact line, we found that the ratio of buoyancy force to capillary force remained relatively constant at 2. Further examination of the bubble growth dynamics revealed a two-stage process involving an expansion stage and an exit stage. Importantly, the underlying physics governing this process still followed the balance between buoyancy force and capillary force, i.e., Tate's law, a theory originally proposed for quasi-steady conditions, whereas the continuous gas injection at the exit stage further increases the bubble size compared to the quasi-static condition.

This research extends the applicability of Tate's law to dynamic bubbling processes using hydrophobic surfaces, enabling the generation of monodispersed bubbles at a wide range of gas flow rates, highlighting the impact of hydrophobic materials on bubble size distribution and the reduction of bubble coalescence. The understanding gained from this study may lead to the development of optimized systems for improved performance in applications such as wet etching, metallurgical processes, and bubble column reactors. Overall, the combination of experimental and theoretical advancements in this work advances our understanding of bubble generation dynamics and opens new avenues for precise control of the bubble size in various engineering and scientific domains.

■ ASSOCIATED CONTENT

Data Availability Statement

During the preparation of this work, the author(s) used ChatGPT to improve the language. After using this tool, the author(s) reviewed and edited the content as needed and take(s) full responsibility for the content of the publication.

Supporting Information

The Supporting Information is available free of charge at https://pubs.acs.org/doi/10.1021/acsomega.3c08187.

Bubble growth process with a orifice diameter of 0.3 mm; 2. Bubble volume analysis method (PDF)

■ AUTHOR INFORMATION

Corresponding Authors

Bo Liu − *Department of Mechanical and Power Engineering, East China University of Science and Technology, Shanghai 200237, China;* orcid.org/0000-0001-6249-3283; Email: boliu@ecust.edu.cn

Qiang Yang − *Department of Mechanical and Power Engineering, East China University of Science and Technology, Shanghai 200237, China*; Email: qyang@ecust.edu.cn

Authors

Hao Zhang − *Department of Mechanical and Power Engineering, East China University of Science and Technology, Shanghai 200237, China*

Haiqiang Yang − *Department of Mechanical and Power Engineering, East China University of Science and Technology, Shanghai 200237, China*

Fang Yuan − *Department of Mechanical and Power Engineering, East China University of Science and Technology, Shanghai 200237, China*

Complete contact information is available at: https://pubs.acs.org/10.1021/acsomega.3c08187

Notes

The authors declare no competing financial interest.

■ ACKNOWLEDGMENTS

This work was financially supported by the National Key Research and Development Program of China (2022YFE0130000-03), National Natural Science Foundation of China (22178099), the Open Project of State Key Laboratory of Chemical Engineering (SKL-ChE-22C02), the Shanghai Natural Science Foundation (21ZR1417000), Shanghai Pujiang Program (21PJ1402000), and the Special Project for Peak Carbon Dioxide Emissions-Carbon Neutrality (21DZ1207800) from the Shanghai Municipal Science and Technology Commission.

■ REFERENCES

(1) Kumar, R.; Kuloor, N. K. The Formation of Bubbles and Drops. In *Advances in Chemical Engineering*, Drew, T. B.; Cokelet, G. R.; Hoopes, J. W.; Vermeulen, T., Eds.; Elsevier, 1970; Vol. *8*, pp 255−368.

(2) Corchero, G.; Medina, A.; Higuera, F. J. Effect of wetting conditions and flow rate on bubble formation at orifices submerged in water. *Colloids Surf., A* **2006**, *290* (1), 41−49.

(3) Pinczewski, W. V. The formation and growth of bubbles at a submerged orifice. *Chem. Eng. Sci.* **1981**, *36* (2), 405−411.

(4) Tan, R. B. H.; Harris, I. J. A model for non-spherical bubble growth at a single orifice. *Chem. Eng. Sci.* **1986**, *41* (12), 3175−3182.
(5) Liow, J.-L.; Gray, N. B. A model of bubble growth in wetting and non-wetting liquids. *Chem. Eng. Sci.* **1988**, *43* (12), 3129−3139.
(6) Yin, J.; Qian, Y.; Ma, Y.; Wang, D. Experimental study on the bubble trajectory in an axial gas-liquid separator applied for tritium removal for molten salt reactors. *Nucl. Eng. Des.* **2017**, *320*, 133−140.
(7) Cervi, E.; Lorenzi, S.; Luzzi, L.; Cammi, A. Multiphysics analysis of the MSFR helium bubbling system: A comparison between neutron diffusion, SP3 neutron transport and Monte Carlo approaches. *Ann. Nucl. Energy* **2019**, *132*, 227−235.
(8) Herrera-Hernández, E. C.; Pérez-Valseca, A. D.; Aguilar-Madera, C. G.; Vázquez-Rodríguez, A. Heat transfer coefficients for bubbly molten salt nuclear reactors. *Nucl. Eng. Des.* **2023**, *414*, 112549.
(9) Huang, Y.-C.; Chen, C.-HWet chemical process tank with improved fluid circulation US 20,020,092,614 A1, 2002.
(10) Abiko, Y.; Kojimaru, T.; Magara, K.; Hiroe, T.; Hasegawa, K.Substrate treating apparatusUS 7,243,911 B2.2007.
(11) Mirsandi, H.; Smit, W. J.; Kong, G.; Baltussen, M. W.; Peters, E. A. J. F.; Kuipers, J. A. M. Influence of wetting conditions on bubble formation from a submerged orifice. *Exp. Fluids* **2020**, *61* (3), 83.
(12) Hecht, K. J.; Velagala, S.; Easo, D. A.; Saleem, M. A.; Krause, U. Influence of Wettability on Bubble Formation from Submerged Orifices. *Ind. Eng. Chem. Res.* **2020**, *59* (9), 4071−4078.
(13) Gnyloskurenko, S. V.; Nakamura, T. Wettability Effect on Bubble Formation at Nozzles in Liquid Aluminum. *Mater. Trans.* **2003**, *44* (11), 2298−2302.
(14) Lesage, F. J.; Cotton, J. S.; Robinson, A. J. Modelling of quasi-static adiabatic bubble formation, growth and detachment for low Bond numbers. *Chem. Eng. Sci.* **2013**, *104*, 742−754.
(15) Lesage, F. J.; Marois, F. Experimental and numerical analysis of quasi-static bubble size and shape characteristics at detachment. *Int. J. Heat Mass Transfer* **2013**, *64*, 53−69.
(16) Tate, T. XXX. On the magnitude of a drop of liquid formed under different circumstances. *London, Edinburgh, And Dublin Philos. Mag. J. Sci.* **1864**, *27* (181), 176−180.
(17) Worley, J. D. Capillary radius and surface tensions. Using calculations based on Tate's law. *J. Chem. Educ.* **1992**, *69* (8), 678.
(18) Riba, J.-R.; Esteban, B. A simple laboratory experiment to measure the surface tension of a liquid in contact with air. *Eur. J. Phys.* **2014**, *35* (5), 055003.
(19) Lee, B.-B.; Ravindra, P.; Chan, E. S. A critical review: Surface and interfacial tension measurement by the drop weight method. *Chem. Eng. Commun.* **2008**, *195*, 889−924.
(20) Hernandez-Aguilar, J. R.; Cunningham, R.; Finch, J. A. A test of the Tate equation to predict bubble size at an orifice in the presence of frother. *Int. J. Miner. Process.* **2006**, *79* (2), 89−97.
(21) Vazquez, A.; Leifer, I.; Sánchez, R. M. Consideration of the dynamic forces during bubble growth in a capillary tube. *Chem. Eng. Sci.* **2010**, *65* (13), 4046−4054.
(22) Earnshaw, J. C.; Johnson, E. G.; Carroll, B. J.; Doyle, P. J. The Drop Volume Method for Interfacial Tension Determination: An Error Analysis. *J. Colloid Interface Sci.* **1996**, *177* (1), 150−155.
(23) Oğuz, H. N.; Prosperetti, A. Dynamics of bubble growth and detachment from a needle. *J. Fluid Mech.* **1993**, *257*, 111−145.
(24) Davidson, J. F.; Schueler, B. O. G. Bubble formation at an orifice in an inviscid liquid. *Trans. Inst. Chem. Eng.* **1960**, *38*, 335−342.
(25) Loimer, T.; Machu, G.; Schaflinger, U. Inviscid bubble formation on porous plates and sieve plates. *Chem. Eng. Sci.* **2004**, *59* (4), 809−818.
(26) Lubetkin, S. Chapter 6 - Bubble nucleation and growth.In *Controlled Particle, Droplet and Bubble Formation*, Wedlock, D. J., Ed.; Butterworth-Heinemann, 1994, pp 159−190.
(27) Fritz, W. Berechnung des Maximalvolumes von Dampfblasen. *Phys. Z.* **1935**, *36*, 379−384.
(28) Lin, J. N.; Banerji, S. K.; Yasuda, H. Role of Interfacial Tension in the Formation and the Detachment of Air Bubbles. 1. A Single Hole on a Horizontal Plane Immersed in Water. *Langmuir* **1994**, *10* (3), 936−942.
(29) Jańczuk, B.; Chibowski, E.; Białopiotrowicz, T. Interpretation of the contact angle in quartz/organic liquid film-water system. *J. Colloid Interface Sci.* **1984**, *102* (2), 533−538.
(30) Balachandran, D.; John, A. Effect of cleaning and storage on quartz substrate adhesion and surface energy. In *Extreme Ultraviolet (EUV) Lithography V*, Wood, O. R., II; Panning, E. M. Eds.; SPIE, 2014. Vol. *9048*, pp 142−148. DOI: .
(31) Deng, Y.; Xu, L.; Lu, H.; Wang, H.; Shi, Y. Direct measurement of the contact angle of water droplet on quartz in a reservoir rock with atomic force microscopy. *Chem. Eng. Sci.* **2018**, *177*, 445−454.
(32) Garstecki, P.; Stone, H. A.; Whitesides, G. M. Mechanism for Flow-Rate Controlled Breakup in Confined Geometries: A Route to Monodisperse Emulsions. *Phys. Rev. Lett.* **2005**, *94* (16), 164501.
(33) Yildirim, O.; Xu, Q.; Basaran, O. A. Analysis of the drop weight method. *Phys. Fluids* **2005**, *17* (6), 062107.

https://doi.org/10.1021/acsomega.3c08187
ACS Omega 2024, 9, 18854−18861